Chapter 1

Introduction and Literature survey

1.1 Introduction

Polycrystalline materials are classified based on their average grain size as coarse-grained (more than 1 μm), ultrafine-grained (between 1 μm and 100 nm), and nanostructured (less than 100 nm) [1–3]. The ultrafine-grained (UFG) and nanostructured materials (NSM) exhibit higher strength and hardness values compared to coarse-grained materials [4]. The properties of materials are mainly influenced by their chemical composition, atomic structure, and crystallite size. The reduction in size has significant effects on the modification of the mechanical and optical properties of materials [2]. If the material is introduced with a significant amount of defects, the volume fraction of the defect cores can become comparable to the volume fraction of the crystalline region. The presence of smaller crystallite sizes and a larger proportion of grain boundaries predominantly contribute to these attributes [1,5]. In materials with reduced crystallite size and a larger grain boundary fraction, there is a significant volume percentage of the grain boundary, and the number of atoms residing nearby increases as the grain size decreases from ultrafine to the nano range [6]. These materials exhibit thermodynamic instability due to their small size. Nanostructured materials possess superior characteristics compared to coarse-grained materials, primarily due to the strong control exerted by interfaces and grain boundaries, which restrict the movement of dislocations. The presence of interphase interfaces further hinders dislocation movement. However, if nanoprecipitates are present in small quantities, they may not exhibit the same characteristics as true nanomaterials. The interfacial area per unit volume (S_V) should be sufficiently large to establish a governing length scale ($\bar{L} = 2/S_V$) of the order 20–50 nm [7]. When the crystal size is made sufficiently big, the strength level is expected to be lower as there will always be an equilibrium number of vacancies and lattice defects in comparison to defect-free material. For this reason, production of bigger dimension material with impressive mechanical properties are difficult.

There are two primary methods available for reducing the grain size of steels to the ultrafine-grained (UFG) or nano level. The first method involves the imposition of severe strain on the specimen, known as severe plastic deformation (SPD) [8]. This process increases the dislocation density and subsequently rearrangement of these defects, leading to the refinement of the microstructure and also improvement in mechanical properties. The SPD techniques include equal-channel angular pressing (ECAP), high-pressure torsion, accumulative roll bonding, and mechanical alloying. Among these techniques, ECAP is widely adopted method for producing bulk samples. The other method is by the isothermal transformation of steel below the pearlite transformation temperature (≈125°C-300°C) to form a nanostructured bainite phase [9,10].

1.2 Equal-channel angular pressing

This process was initially developed by Segal and his colleagues in the 1980s [11]. However, ECAP process was not so popular during its early stage of development within the scientific community. This situation started to change in the 1990s, highlighting the potential of ECAP for producing metals with ultrafine-grained and submicrometric structures, leading to the development of new and unique material properties [12].

The process of metal flow during ECAP process [11,13] is illustrated schematically in Figure 1.1. The die features an internal channel that is bent at an abrupt angle ϕ of 120°. There is an additional angle ψ (outer arc of curvature where the two channels intersect) of 60° as shown in Figure 1.1 [14]. Usually, the sample takes the form of a rod or bar that is prepared to fit within the channel. The die is positioned within a press setup, enabling the sample to be pressed through the die using a plunger. The predominant form of deformation imposed is simple shear, which takes place as the sample traverses through the die. Shear plane in ECAP is the

deformation plane of the sample aligned at half of intersection angle (ϕ). This is different from crystallographic slip plane.

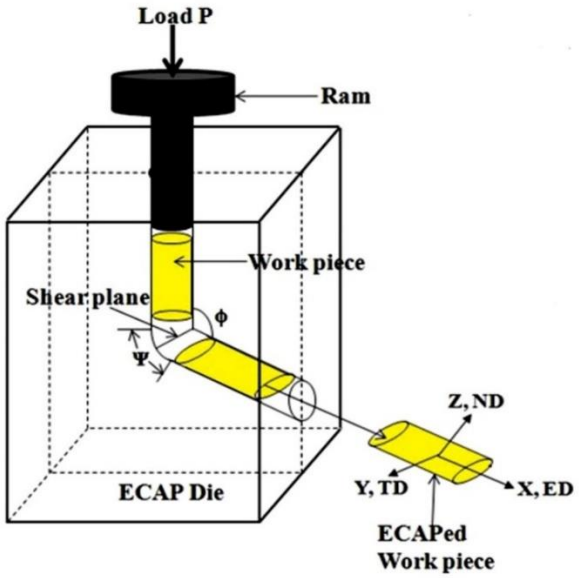

Figure 1.1. *ECAP die assembly with intersection angles of φ and ψ along with reference directions* [14].

Even though the sample experiences significant strain, when it passes through the die and deforms through the shear plane of the sample, the cross section remains unchanged. A distinguishing feature of SPD processing is its ability to maintain the same cross-sectional area throughout the process, even when subjected to significant strains. This characteristic distinguishes it from conventional metal-working methods such as rolling, extrusion, and drawing. Due to the consistent cross-sectional area, the sample can undergo repeated pressing, facilitating the accumulation of remarkably high strains.

1.2.1 The strain imposed in ECAP

During the ECAP process, strain is exerted on the sample with every pass through the die. The magnitude of this strain can be analytically estimated, considering the configurations illustrated in Figure 1.1. In the figure, the channel angle is marked as Φ, while the angle ψ signifies the intersection of the two segments of the channel [15]. To estimate the shear strain

(Υ), it is assumed that the sample is fully lubricated, allowing frictional effects to be neglected. The equation for estimating the shear strain is given in the Equation 1.1.

$$\Upsilon = 2 \cot\left(\frac{\psi}{2} + \frac{\Phi}{2}\right) + \psi \operatorname{cosec}\left(\frac{\psi}{2} + \frac{\Phi}{2}\right) \quad (1.1)$$

After N passes, the equivalent strain (ε_N), can be expressed by the relationship given in Equation 1.2.

$$\varepsilon_N = \frac{N}{\sqrt{3}}\left[2 \cot\left(\frac{\psi}{2} + \frac{\Phi}{2}\right) + \psi \operatorname{cosec}\left(\frac{\psi}{2} + \frac{\Phi}{2}\right)\right] \quad (1.2)$$

1.2.2 The fundamental processing routes in ECAP

The ECAP process is categorized into four distinct routes, each introducing a unique slip system during the pressing procedure. This results in a notable diversity in the resulting microstructures [16,17]. Figure 1.2 provides a schematic summary of these four processing routes. In route A, the sample undergoes pressing without any rotation. In route B_A, the sample is rotated by 90° in alternating directions between consecutive passes. In route B_C, the sample is rotated by 90° in the same direction (either clockwise or counterclockwise) between each pass. In route C, the sample is rotated by 180° between passes.

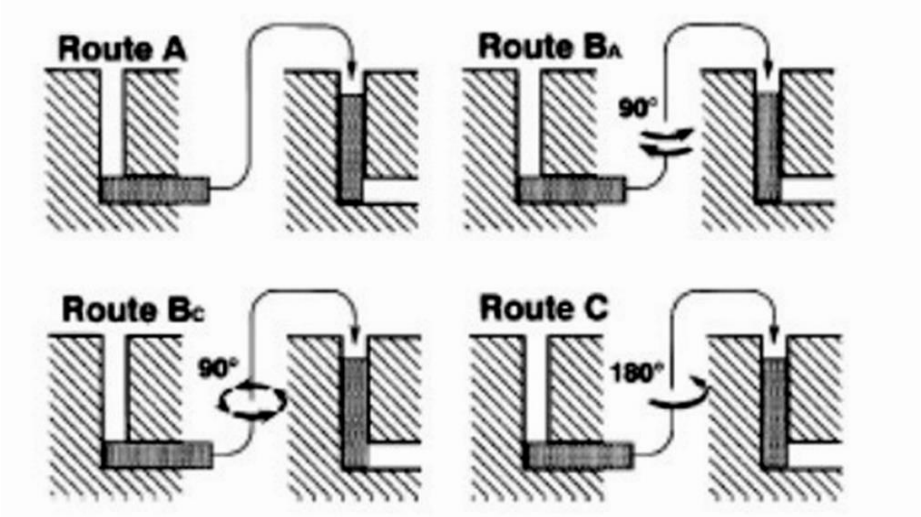

Figure 1.2. *Schematic diagrams showing fundamental processing routes of ECAP* [16].

1.2.3 Strain development in different processing routes

The schematic diagram in Figure 1.3 depicts the distinct slip systems linked to each processing route. In this illustration, the X, Y, and Z planes signify the three orthogonal planes, displaying slip for various passes within each processing route. The labelled planes 1 through 4 correspond to the initial 4 passes of ECAP. Within route C, shearing takes place on the identical plane during each successive passage through the die, though with a reversed shear direction in each pass. Hence, route C is a redundant strain process, as the strain reverts after every even number of passes. Similarly, route B_C also is a redundant strain process. The slips occurring in the first pass are counterbalanced by those in the third pass, and the slips in the second pass are nullified by those in the fourth pass. Conversely, routes A and B_A are not redundant strain processes. In route A, two distinct shearing planes intersect at a 90° angle, whereas in route B_A, four separate shearing planes intersect at angles of 120°. In both routes A and B_A, there's a progressive accumulation of additional strain with each successive pass through the die.

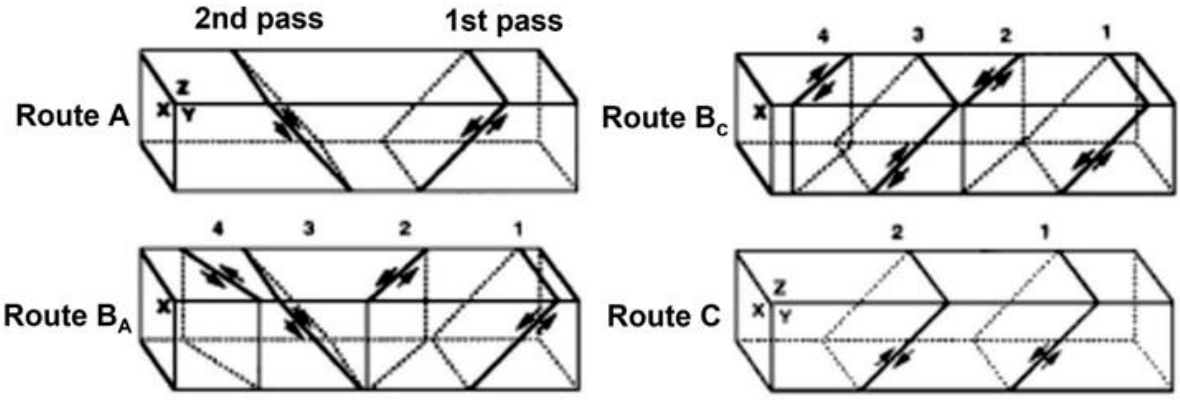

Figure 1.3. *Schematic diagram showing strain development with each pass of ECAP using processing routes A, B_A, B_C and C* [18]

1.2.4 Microstructure and mechanical properties of ECAPed material

In the ECAP process, the application of severe plastic strain to the specimen causes an increase in dislocation density without causing any external shape change. The dislocation structures within the material consist of incidental dislocation boundaries and geometrically necessary boundaries (GNB) [19]. As the strain increases, the GNB undergo several steps of evolution. First, they reorganize into deformation bands. Then, the spacing between these bands reduces to a cell size. Following this, the GNB rotate towards the overall flow direction, causing an elevation in the misorientation angles [20,21]. These concurrent alterations in microstructure and texture can lead to either material hardening or softening, contingent upon the particular material and mode of deformation. As strains grow substantial, the hardening effect might steadily persist. Conversely, at moderate strains, softening can intervene, causing localized flow disruptions. If softening takes precedence, the ongoing evolutionary process transitions into flow localization within shear bands. Shear bands are narrow, planar layers within the material that accommodate notably higher strains compared to their surrounding regions. The average spacing between shear bands approximates the cell size seen outside these bands. Crystallographic multi-slip activity inside shear bands results in increased misorientation angles along their boundaries. Shear bands come into existence by substituting pre-existing structures and ultimately define the ultimate configuration of intensely deformed metals. Across the deformation process, the original grains undergo extensive subdivision, and fresh boundaries emerge based on the misalignment among lattice orientations of volume components. As deformation advances, the degree of misalignment varies, and the gaps between these boundaries continuously shrink. Through the realignment of these imperfections, the microstructure undergoes refinement, leading to enhancements in mechanical properties. In the initial passes, low-angle grain boundaries (LAGB) develop, and the microstructure with shearing becomes visible under an optical microscope. However, at

higher passes, LAGB arrange into high-angle grain boundaries (HAGB). In various experiments conducted on low carbon steel, researchers have investigated the evolution of microstructural and mechanical properties using ECAP [22–24]. Shin et al. applied ECAP to a commercial low carbon steel, achieving an equivalent strain of 4 and producing elongated grains with a size of 0.2-0.3 μm [22]. Another study by Fukuda et al. focused on ECAP of 0.08 mass% carbon steel using the B_c route. They observed that the first two passes predominantly produced LAGB, which were then converted to equiaxed HAGB of approximately 0.2 μm after three passes [24]. The resulting steel exhibited ultimate tensile strength (UTS) exceeding 800 MPa, but the ductility was reduced compared to the base material. Singh et al. conducted extensive research on ECAP of low carbon steel using the B_c route across a range of passes, from low to high [14]. They found that, the maximum grain size reduction can be reduced up to 0.2 μm, after ε_{vM} of 6. Average grain size does not decrease on increasing number of passes rather saturation is observed. Similarly, HAGB fraction is increased up to ε_{vM}=6 and on further pressing more LAGB is created, aiding in the strength enhancement seen in their work.

Figure 1.4 depicts the plot of yield stress against grain size (in μm) for bcc steels processed via various routes [25]. The ultrafine microstructures result from the SPD methods are shown by open symbols. The yield stress of the steel follows the Hall–Petch relationship, as presented in Equation 1.3.

$$\sigma_y = \sigma_i + K_y d^{-1/2} \qquad (1.3)$$

where σ_y is the yield stress, σ_i the friction stress, K_y the grain boundary resistance and d is the grain size. It is clear from Fig. 1.4 that UFG produced by SPD techniques follow Hall–Petch relationship and yield strength increases with decrease in average grain size.

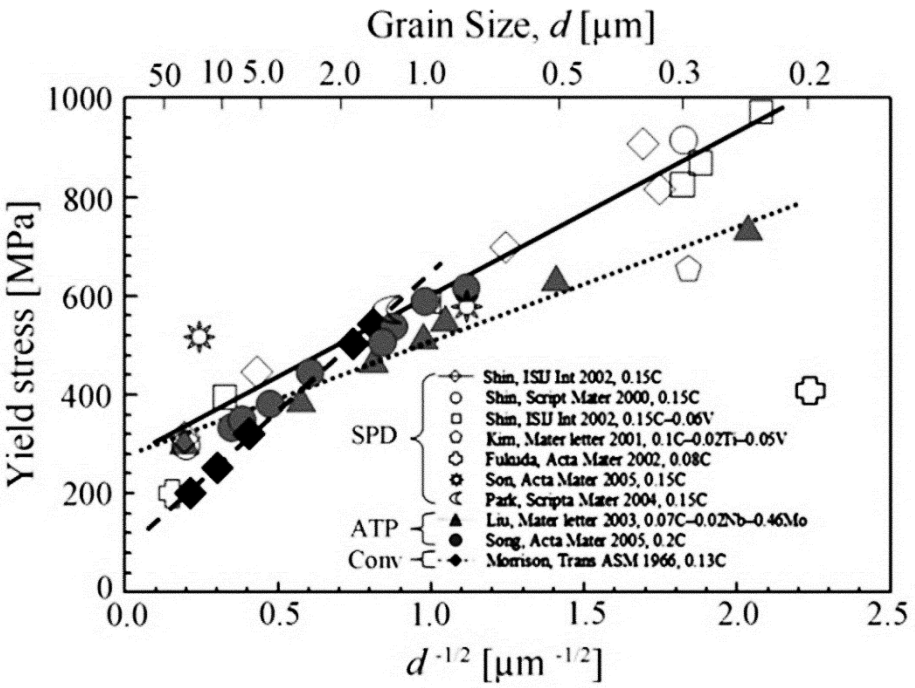

Figure 1.4. *Different steels showing Hall–Petch relationship* [25]. *(Open symbols are for SPD materials, 'ATP' represents advanced thermomechanical processing and 'Conv' stands for conventional).*

Factors such as work hardening and strain rate sensitivity [26] influence the ductility of a material, with higher values of these properties being advantageous for improved ductility. Pile up of defects near grain boundaries is mainly responsible for work hardening. However, in ultrafine or nanostructured materials, the pile-up of dislocations is not feasible due to the reduced mean free path for dislocation movement. A plot of tensile elongation versus the inverse square root of grain size (d) within the range of 150 to 0.2 μm (Fig. 1.5) demonstrates a decrease in elongation as the grain size decreases [25]. Steels subjected to ECAP processing, resulting in grain sizes within the ultrafine range, demonstrate elevated yield strength (YS) but diminished ductility in comparison to the base material [24,27]. The material achieves its highest ductility when the grain size falls within the range of 10-1 μm. Therefore, there is a possibility of recovering ductility in SPD materials by introducing a proportion of fine grains alongside the majority of ultrafine grains through further processing.

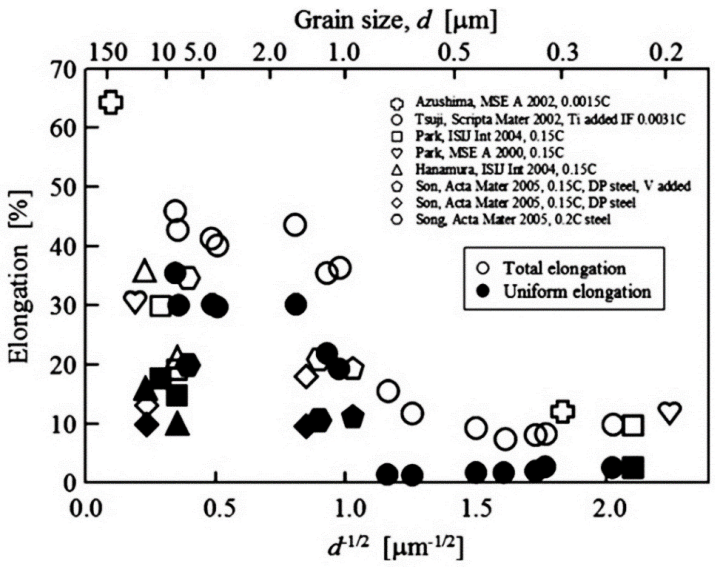

Figure 1.5. *Variation in ductility with grain size for bcc steels. Open and filled symbols represent total elongation and uniform elongation in tension respectively* [25].

Yinmin Wang et al. [28] introduced a short time annealing method to restore ductility in the ultrafine grained SPD materials. Through annealing for only 3 minutes at 180 °C, they were able to achieve ductility levels comparable to the base material, while maintaining a significant portion of the strength, as illustrated in Figure 1.6a. This short-duration annealing process led to the abnormal growth of some grains, while others remained in the nano-sized range, as depicted in Figure 1.6b. The presence of finer grains contributed to the material's strength, while the micron-sized grains facilitated enhanced strain hardening. Similar findings have been reported by other researchers [29,30] in their respective studies.

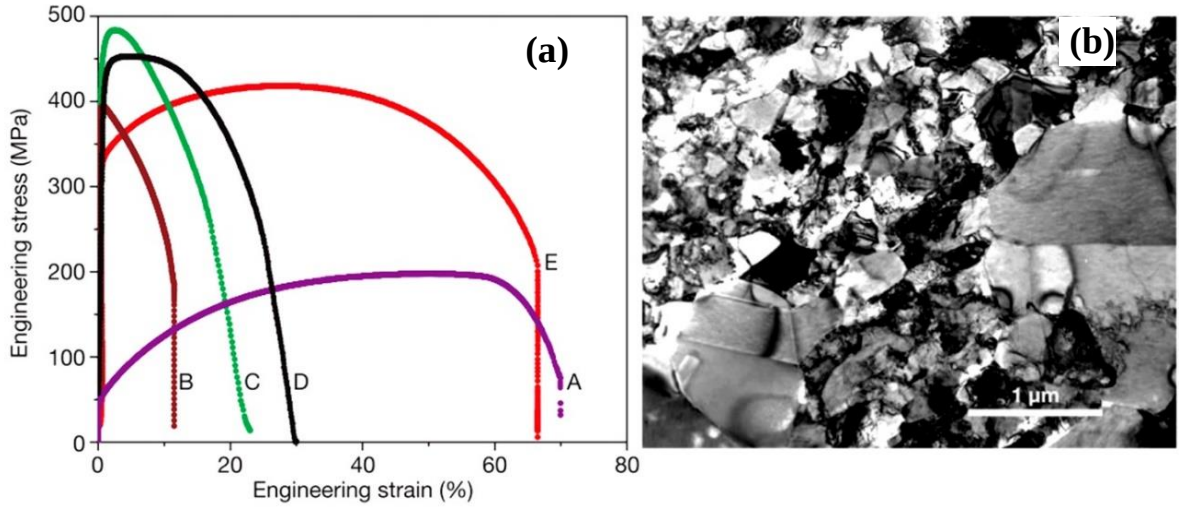

Figure 1.6.*(a) Engineering stress–strain plots for pure Cu. (Plot A is annealed, coarse grained Cu; B is 95% cold worked (CW) at room temperature; C is 93% CW at liquid-nitrogen temperature; D is 93% CW +180° C for 3 min.; and E, 93% CW +200° C, 3 min (b) TEM BF image of condition E showing bimodal grain distribution* [28].

While short-time annealing has shown promise in recovering ductility to some extent in ultrafine-grained SPD materials, there are certain limitations to this approach. One such limitation is the irregular nature of the micron-sized grains that result from the abnormal growth during annealing. This uneven grain growth has the potential to cause a reduction in tensile strength. Furthermore, the annealing process itself requires extra processing time and could lead to increased energy consumption, which could be a practical concern.

1.3 Electropulsing

The Electropulsing (EP) technique involves applying a high-density electric current pulse lasting from microseconds to milliseconds to a specimen, which can be metallic, ceramic, etc. The specimen is positioned between conducting electrodes, allowing for rapid cooling after heating due to Joule heating. The main advantages of EP are its high efficiency, time-saving nature, and cost-effectiveness. In recent times, the impact of electric current on various solid-state transformations in metals has gained significant importance in research, including: (1) improvement in plasticity [31,32] (2) crystallization of amorphous alloys [33,34], (3) accelerated recrystallization and restricted grain growth followed by cold working [35–37], (4) nanocrystallization [38,39] and the like.

The concept of electropulsing treatment (EPT) was initially introduced in the 1960s by a Russian scientist who conducted experiments involving the electron radiation-assisted drawing of a single crystal of Zn [40]. During these experiments, it was noted that an elevation in electron radiation resulted in a reduction in drawing stress [31]. Subsequently, Okazaki [41] observed that titanium wires subjected to current pulses within the range of 0 to 8000 A/mm^2 exhibited stress relaxation during the pulses under constant-strain-rate conditions. Following

these observations, the applications of EPT have flourished within the domains of materials science and engineering.

1.3.1 Electroplasticity

The initial experiments on EP focused on improving the plasticity of materials. Machlin [40] pioneered the application of a 6 kV DC to a rock salt crystal, noting a decrease in YS and an increase in elongation compared to the sample without current. Subsequently, Troitskii [31] applied pulsed current to different metals undergoing uniaxial tensile deformation at a constant strain rate. They noted pronounced serrations in the stress-strain curves, accompanied by a significant reduction in flow stress, as illustrated in Figure 1.7. Their observations revealed that the decline in flow stress per current pulse was influenced by voltage and the count of current carriers. No noticeable impact of current pulses was evident in the elastic region, and the abrupt shifts in flow stress manifested exclusively in the plastic region. This observation implied a strong connection with dislocation motion. This phenomenon was consequently termed the "electro-plastic effect. Okazaki et al. [41] reported similar observations when applying electric current pulses up to 8000 A/mm^2 during uniaxial tension. They noted a decrease in the load within the load-elongation curve as a consequence of electropulsing, and the extent of this drop amplified with higher current density. They proposed that this load drop might be attributed to electron-dislocation interaction.

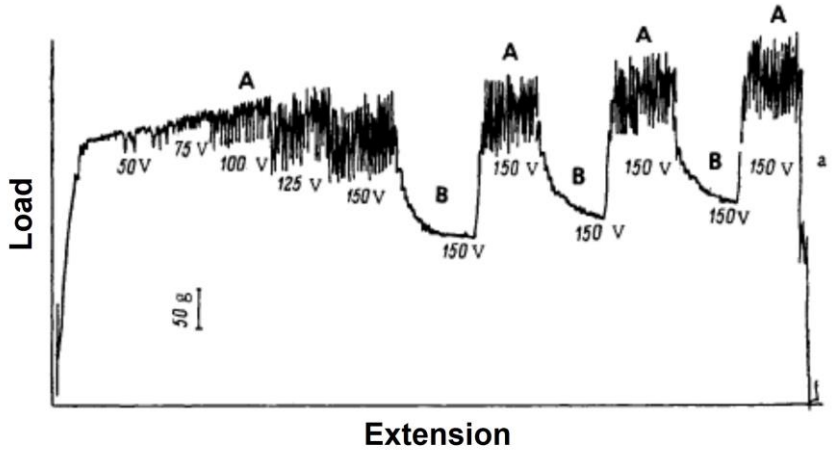

Figure 1.7. *Load vs. extension plot of a zinc single crystal at 78K during the application of a DC pulse (100V – 1.5 x 10^5 A/cm^2)*

Spreacher et al. [42] conducted experiments involving the application of DC current pulses to various materials under uniaxial tension. Their findings supported the observations proposed by Troitskii and Okazaki. Additionally, they discovered that elastic strain resulting from thermal expansion due to Joule heating played a role, while effects such as skin, pinch, and magnetostriction had minimal importance. They substantiated the interaction between electron wind force and dislocations as the underlying cause of the load drop during plastic deformation. They found estimated push coefficient (~10^{-4} dynes/cm^2) from the electron wind force in metals is higher (~ an order of magnitude) than that of electron drag coefficient (~10^{-5} dynes/cm^2) determined from the measured dislocation velocity

During EP, the temperature of the deformed material remains lower than what is predicted by Joule's law of electric heating. The threshold current density value, governing the load increase, diminishes as the degree of plastic deformation in the material rises. The plastic deformation of metals during EP transpires owing to the direct transfer of energy from the conduction electrons to the dislocations [43].

Recent studies on Ti-7Al [32] alloy have demonstrated that the application of EP can induce defect reconfiguration, transforming the planar slip observed in the deformed material (Figure

1.8a) into wavy slip (Figure 1.8b). This change in slip behaviour increases the ductility of the material.

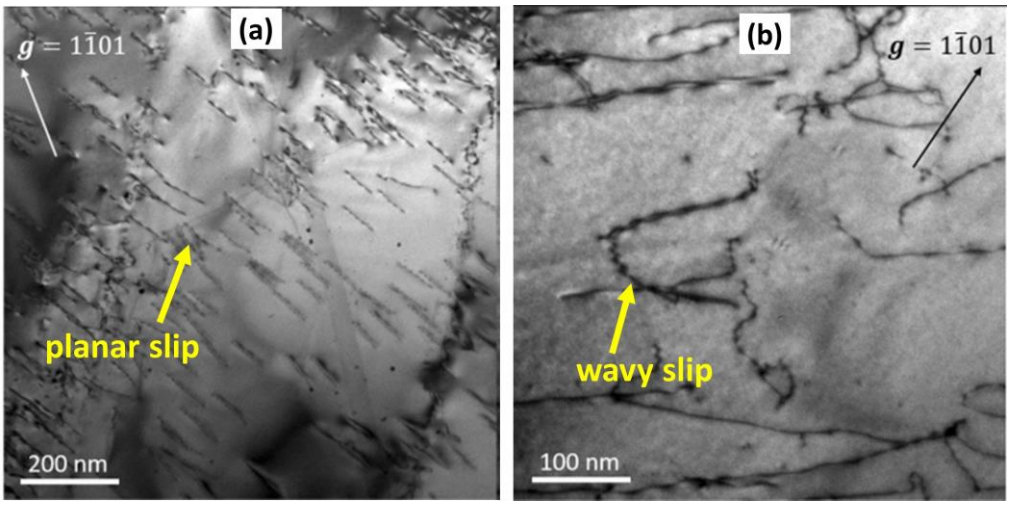

Figure 1.8. *Ti-7Al subjected to 2% of plastic strain at room temperature (a) without pulsing and (b) after pulsing* [32].

1.3.2 Accelerated recrystallization

Numerous researchers have provided evidence that EP treatment can expedite the process of recrystallization by enhancing the nucleation rate [37,44,45]. For instance, when a cold-worked brass undergoes recrystallization at temperatures of 570 °C and 650 °C for 30 minutes, the resulting optical microstructures reveal the formation of coarse grains, as depicted in Figures 1.9a and b. However, when EP is applied at a current density of 17 kA/mm^2 for 800 µs, smaller recrystallized grains are formed compared to conventional annealing treatment, as shown in Figure 1.9c [46]. Additionally, the yield strength in this process increases from 113 MPa in the case of annealing at 570 °C to 214 MPa with the application of electropulsing. Due to high current density the drift electrons exert a force on the dislocations, leading to their accelerated movement and refinement of grains within short period of time.

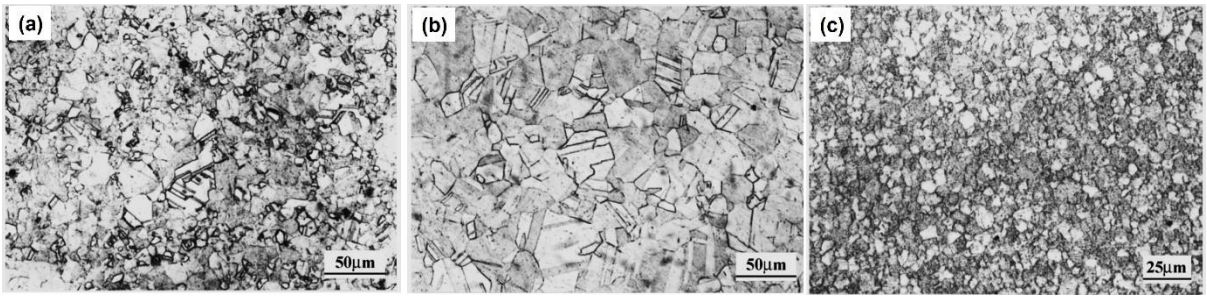

Figure 1.9. *Optical micrographs of a cold worked brass after annealing at (a) 570^0 C, (b) 650^0C and (c) after electropulsing treatment* [46].

1.3.3 Nanocrystallization

In the research conducted by Zhou et al. [47], a high-density current pulse is administered to a normalized low carbon steel featuring an initial grain size of 6 μm (Figure 1.10a). The EPT employs a current density of 10.5 kA/mm^2 for a cumulative duration of 800 μs. The resulting microstructure exhibited a bimodal distribution, with smaller grains measuring around 40 nm and larger grains of 6 μm (Figure 1.10b). During this process, the temperature rise reached approximately 1000 °C. The tensile strength and elongation of the material are significantly increased, as demonstrated in Table 1.1, which has garnered considerable attention for the electropulsing treatment process.

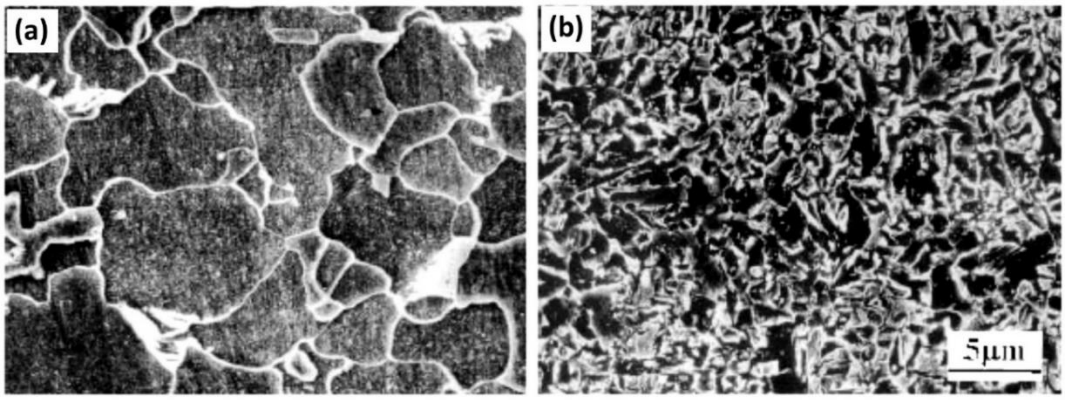

Figure 1.10. *SEM micrographs (a) Austenitization at 950 °C for10 min followed by air cooling and (b) electropulsing of air-cooled sample at 10.5 kA/mm^2* [47].

Table 1.1. Mechanical properties of samples, with and without electropulsing [47].

Sample	Tensile strength (MPa)	Elongation (%)	Micro hardness (HV)
Heat treated sample	580	40	179
Electropulsed sample	1040	45	325

Accelerated nucleation and grain refinement during rapid heating and cooling are primarily responsible for the nano crystallization process. In the heating cycle, fine γ grains form but do not have sufficient time to grow due to the rapid heating. Similarly, during the cooling cycle, α grains form within the γ grains, but they also lack sufficient time to grow due to the rapid cooling as schematically shown in Figure 1.11 [47].

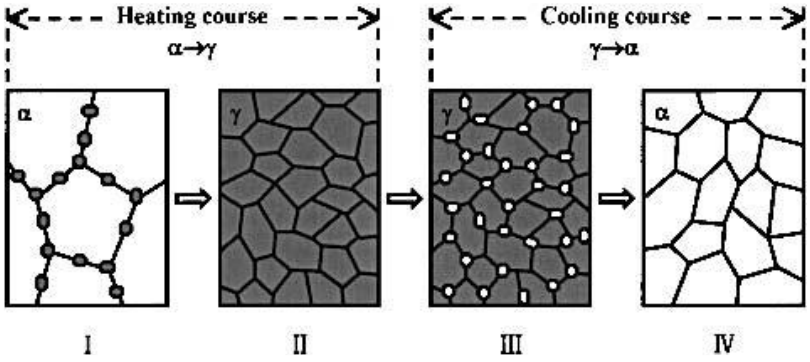

Figure 1.11. *Schematic diagram illustrating grain refinement (I) formation of γ-phase nuclei, (II) formation of γ -phase grains by the growth of nuclei, (III) α-phase nuclei formation during cooling and (IV) formation of α -phase grains by the growth nuclei* [47].

In the study conducted by Du et al. [48] on a Cu-Zn alloy, they observed similar types of nanocrystalline structures. By applying a current density of 12.8 kA/mm^2, they were able to generate a temperature of 900 °C, which was sufficient to melt the surface of the sample. The researchers also calculated the skin depth and temperature distribution along the depth and discovered that as the thickness increased, the temperature and current decreased. Additionally, they found that the degree of refinement decreased from the nano to micron scale as the thickness increased. The rapid heating and cooling, coupled with the enhanced nucleation rate prompted by EP, led to the creation of nanocrystalline structures within the sample.

In the case of 22MnB5 boron steel [39], local nanostructured γ phase was observed after applying a pulse current of 890.1 MA/mm^2 for 100 ms. While ferrite and pearlite phases are stable at room temperature, the formation of the gamma iron phase occurs locally due to the absence of long-range diffusion.

1.3.4 Qualitative hypotheses on electropulsing

All of the work referred to above accepts that combination of thermal (due to local temperature rise) and athermal effects are responsible for the observed changes. The foundational theory proposes that EP enhances the mechanism of sub-grain coalescence by augmenting the mobility of dislocations. This, in turn, influences the rate of nucleation for new strain-free grains. This improvement in dislocation mobility is attributed to the additional force provided by the electron wind, which acts on dislocations in the material and contributes to heterogeneous electromagnetic shielding. The electron wind force assists dislocations in overcoming obstacles during their motion, providing an extra push. Consequently, the decrease in dislocation density and the increased mobility of dislocations, facilitated by the electron wind force, amplify the nucleation rate of recrystallization. This process ultimately yields a refined microstructure.

In recent research by Jeong et al. [49] the emphasis was placed on discerning the individual impacts of thermal and athermal effects on the kinetics of recrystallization in ultra-low carbon steel. The study revealed that the athermal effect plays a major role compared to the heating effect. Specifically, below a current density of 70 A/mm^2, there was a decrease in the recrystallization and grain growth. However, above this current density, there was an increase in recrystallization and grain growth, following a V-shaped trend as depicted in Figure 1.12. Their findings indicate that the athermal effect has a significant influence on the recrystallization kinetics of the material, surpassing the impact of heating alone. With

increasing current density, the athermal part of the pulse reduces the activation energy for recrystallization. On the other hand, temperature rises with current density, but its effect is relatively lower as the material experiences shorter time to this elevated temperature.

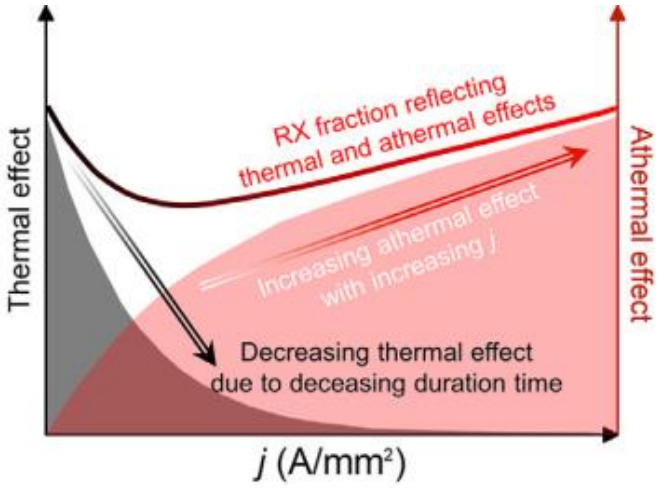

Figure 1.12. *The schematic diagram illustrates the thermal and athermal effects change in relation to the current density.* [49].

1.4 Transformations in steel

Properties of steel can easily be altered due to the possibility of phase transformations occurring at different temperatures in the solid state. The phase diagram and phase transformation behavior are significantly influenced by the presence and composition of alloying elements. In most heat treatments, the steel is heated into the single-phase austenite (γ) region. When the Fe-C steel (with a carbon content below 0.76 mass%) is slowly cooled to ambient temperature, ferrite (α) and perlite are formed.

The products formed during the cooling of austenite to room temperature are classified into two categories: reconstructive and displacive transformations. Reconstructive transformations occur at relatively elevated temperatures where atomic diffusion holds significance. During a reconstructive transformation, atoms move randomly, and there is no atomic correspondence between the parent and product phases. The long-range diffusion of atoms aims to minimize

the strain energy, resulting in no observable change in shape. Examples of reconstructive transformations include allotriomorphic ferrite, idiomorphic ferrite, and pearlite.

On the other hand, displacive transformations occur at low temperatures where diffusion is impossible within the time scales involved. The characteristic feature of displacive transformations is the coordinated movement of atoms, preserving the atomic correspondence between the parent and product phases. This leads to a macroscopic shape change, such as a surface uphill, in the sample. The displacive product phase grows in the form of plates to reduce the strain energy associated with the transformation. Examples of displacive transformations include martensite, Widmanstaetten ferrite and bainite.

1.5 Bainitic transformation

Bainite like microstructure was first reported in steel in 1920 by Hultgreen [50], subsequently by Robertson in 1929 [50a] and by Bain and Devenport in a famous article in 1930 [50b]. The word 'bainite' was coined in 1934 in honour of Dr. E. C. Bain to describe the non-lamellar aggregate of ferrite and carbide [50c]. The first recorded citation of the word ''bainite'' is in an article [50d] published 12 years after Davenport and Bain introduced isothermal transformation as a technique to study the progressive evolution of phases as a function of time and temperature. The heat treatment is performed between the completion of the pearlitic transformation and above the martensite start temperature (Ms). Bainitic steel later garnered increased attention compared to martensite due to non-requirement of large cooling rate for large components.

1.5.1 Theories related to bainitic transformation

The theories surrounding bainitic transformation still remain a topic of controversy. One theory, proposed by Hehemann and others [51,52] is based on the theory of martensitic transformation developed by Bain [53]. According to this theory, the nucleation of bainite takes

place in a paraequilibrium manner, involving solely the diffusion of carbon and excluding the diffusion of substitutional elements. However, during the growth of bainite, the transformation is completely diffusionless. Carbon is subsequently partitioned into retained austenite (RA) after the growth of bainite laths/plates, in order to reduce the stored energy associated with the transformation. During the transformation, the austenite is converted into lenticular plates called sub-units, which then come together to form a sheaf-like structure. The major evidences in the support of this theory are (a) No partition of substitutional alloying elements during and after transformation [54] (b) Surface relief measurements through atomic force microscopy [55], (c) Identification of a substantial dislocation density within the RA, as observed by techniques like transmission electron microscopy (TEM), atom probe tomography (APT), and dilatometry. This points toward plastic accommodation due to transformation strains originating from a displacive transformation [56,57].

The second theory, proposed by Aaronson [52] and Hillert [58] supports to the idea that bainite growth occurs via a ledge-propagation mechanism. According to this theory, the pace of bainite growth is governed by the diffusion of carbon preceding the transformation interface. Both nucleation and growth occur under paraequilibrium conditions, similar to the formation of Widmanstätten ferrite. There are several pieces of evidence that support the paraequilibrium ledge-growth mechanism. Firstly, directly observed growth velocities of bainite are more consistent with diffusion velocities rather than displacive transformation velocities [59,60]. This observation suggests that carbon diffusion plays a crucial role in the growth process. Additionally, measurements using scanning tunneling microscopes and atomic force microscopes have revealed surface relief patterns that are more indicative of ledge-wise growth, as opposed to diffusionless growth [61,62].

Certain pieces of evidence favouring the ledge-wise growth mechanism, rooted in the observation of low growth rates under optical microscopy, can also be accounted for by the

rapid growth of sub-units of bainitic ferrite resulting from slow nucleation. The study conducted by Yada et al.[59], which involved in-situ transformation using hot stage microscopy, might not have possessed the resolution necessary to distinguish individual sub-units. The measurements obtained could have pertained to the growth of a packet rather than individual sub-units. Similarly, a study conducted by Kang et al.[63] employed hot-stage TEM to observe the growth of bainite sub-units. Their findings indicated that the growth occurred through shear rather than the ledge-wise mechanism.

Based on these findings, it becomes evident that the diffusionless growth mechanism holds validity for bainite formation. This mechanism bears noteworthy implications for the future design of new compositions and understanding the microstructural evolution in steel.

1.5.2 Cementite precipitation in bainite

Bainitic transformation is generally classified as upper and lower bainite based on carbide precipitation [64]. Upper bainite is generally formed at high temperatures (~300°C–450°C), resulting in the partition of excess carbon into RA without precipitating inside bainite plates. The saturated carbon in RA subsequently comes out in the form of precipitates. The lower bainite is formed in the temperature range (~200°C–350°C). The low transformation temperature leads to slower diffusion and helps in some carbon to precipitate inside bainite plates whereas in RA between plates contain less amount of carbide.

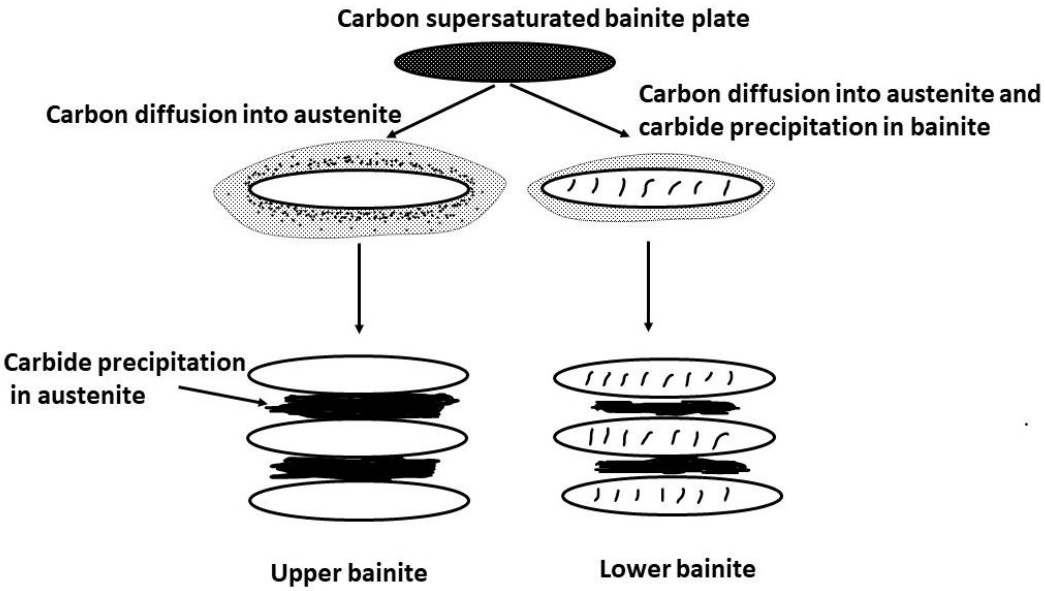

Figure 1.13. *schematic diagram explaining carbon movement and carbide precipitation* [64].

1.5.3 Carbide-free bainite

Earlier bainitic steels suffered from poor ductility due to the presence of brittle carbides in the material. However, the addition of approximately 2 mass% silicon has been found to improve ductility and fracture toughness in bainitic steels [65]. Silicon facilitates the formation of graphite in cast irons by providing electron density to iron atoms. This action inhibits their interaction with clusters of carbon atoms, thereby enabling the carbon atoms to precipitate and form graphite [66].

The mechanism through which silicon restrains the precipitation of cementite has been postulated as follows: Silicon could potentially partition in advance of a growing carbide, accumulating in the area preceding the growth interface. The presence of silicon in this region prevents its incorporation into the carbide lattice. Furthermore, silicon increases the activity of carbon in the austenite, leading to a deceleration in the diffusion of carbon into the carbide. In order for the carbide particle to continue growing, silicon must diffuse away from the interface. Since silicon diffusion is slower in comparison to carbon diffusion, it becomes the constraining factor that hinders the further growth of the carbide. It is assumed that cementite forms initially

under paraequilibrium conditions, without partitioning for substitutional alloying elements, including silicon [67–69]. The thermodynamic effects of incorporating silicon into the cementite lattice are investigated by Bhadeshia et al. [66] and from first principles by Jang et al. [70]. Their research indicated that substituting an iron atom with a silicon atom in the least unfavourable lattice site elevated the enthalpy of cementite formation from around 20 kJ/mol to 120 kJ/mol. This alteration provides a thermodynamic rationale for the soppression of cementite by silicon, as the driving force behind cementite precipitation is notably diminished. The equilibrium calculation of cementite precipitation from the austenite phase containing Fe-1C-1.41Si-1.42Mn (mass %), austempered at 360 °C, as shown in Figure 1.14, indicates that even with a longer period of austempering, no cementite precipitation occurs. This suggests that the presence of silicon in the alloy composition effectively inhibits the precipitation of cementite [66].

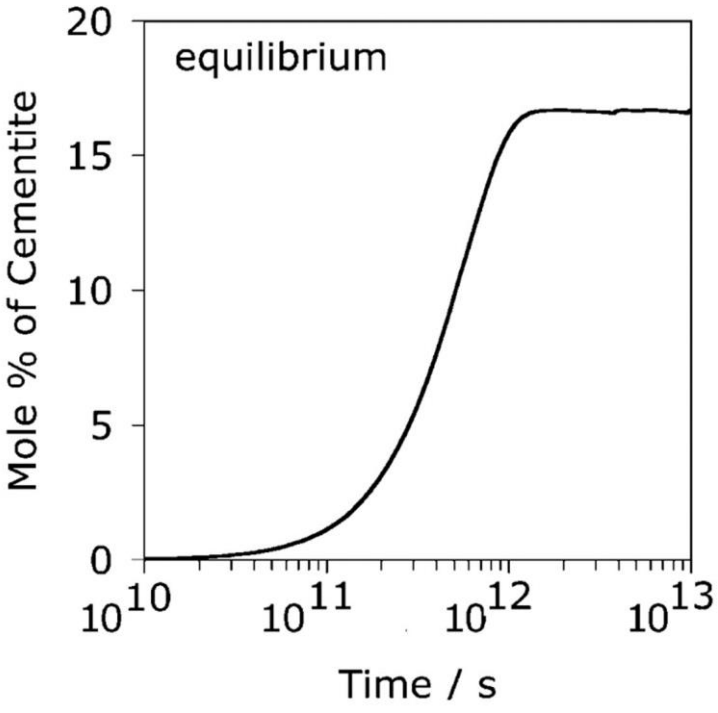

Figure 1.14. *Calculation of cementite formation rate from austenite at 360 °C* [66]

1.5.4 Nanostructured bainitic steel

Nanostructured bainitic steel is first developed by Cabellaro et al. [71] by isothermally transforming high carbon low alloy steel at a temperature of 125°C. Later it is found that nano structured bainite can be produced up to 300 ℃ [72]. The structure of this type of steel is an alternate mixture of bainite plates (less than 100 nm thickness) and films of retained austenite, (~ 50 nm thickness) along with blocky retained austenite (more than 1 µm size) as shown in the TEM BF image in Figure 1.15. Bainitic steels that undergo transformation at low temperatures showcase remarkable combinations of strength and toughness [73]. Due to simple heat treatment process, bulk quantity of nanostructured material can be produced with good mechanical properties. At the same time, low cost of alloying elements to produce bainitic steel and simple processing condition makes this steel economical. Due to the said economic factors and excellent mechanical properties, production of commercial bainitic steel has started for Rail, armour and bearing etc [74].

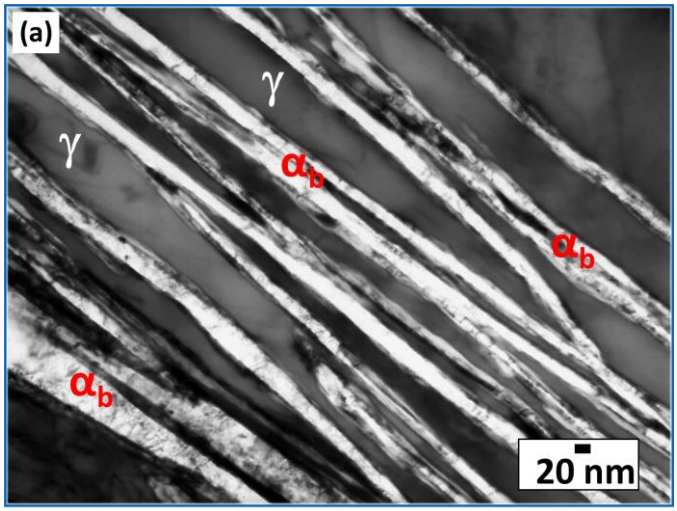

Figure 1.15. *TEM BF image showing nanostructured bainite and retained austenite in between* [71]. *(α_b is bainite and γ is austenite).*

The high strength exhibited by bainite is largely attributed to its fine plates [75,76]. The thickness of bainite plates increases with an increase in the driving force ($\Delta G^{\gamma\rightarrow\alpha}$) and temperature of transformation, but decreases with an enhanced yield strength of austenite (σ^{γ})

[77,78]. Empirical equations have been developed to estimate σ^{γ}, taking into account the contributions from alloying elements, frictional stress, and the size of the austenite grain (d^{γ}) [79,80]. There is ample evidence indicating that bainite undergoes plastic accommodation within the austenite phase during transformation at higher temperatures [77,81]. Bhadeshia and Edmonds have shown that the dislocation density in bainite is higher than in austenite [82], and it has been observed that thinner bainite plates tend to have higher dislocation density [83]. Dislocations generated in austenite during the plastic accommodation process can contribute to the refinement of bainite plates by increasing the yield strength of austenite. Therefore, the dislocation density in the austenite phase is believed to play a crucial role in controlling the thickness of bainite plates.

1.5.5 Orientation relationship and variant pairing

The study of the crystallographic features of bainitic steel is useful as they have a significant impact on the material's toughness and ductility [84–86]. Diffusionless transformation products, such as bainite, exhibit a specific orientation relationship with the parent phase [75]. The OR can be either Kurdjumov–Sachs (K-S) [47] or Nishiyama–Wasserman (N-W) [87] type (Table 1.2), depending on the processing conditions [88]. However, in reality, neither K-S nor N-W relationship is strictly followed since the transformation product is a lattice invariant line instead of a plane, which produces an OR of high index planes [75].

A single austenite grain can give rise to 24 variants of bainite, and the misorientation angle between variant 1 (V1) and the other variants are given in Table 2. In the cubic crystal system, there are four {111} austenite close-packed planes, and for each (111) plane, three orientations $<1\bar{1}0>$ are possible, as shown in Figure 1a. The close-packed plane and direction for bainite are {110} and $<1\bar{1}1>$, respectively. For each γ $<1\bar{1}0>$, there are two ways α_b $<1\bar{1}1>$ can be

aligned, resulting in six variants known as the close-packed (CP) group [89] (Figure1.16a). Since there are four {111} planes in the cubic crystal system, a total of 24 variants are possible for a single austenite grain (V1-V24) [90] (Table 1.3).

Another important orientation relationship that relates bainite to austenite is the Bain orientation, as shown in Table 1.2. Three different Bain groups are present, each associated with eight K-S variants. The misorientation angle between variants within the same Bain group is small. In bainitic steel, a single austenite grain is subdivided into packets, blocks, and laths, similar to martensite, as depicted in Figure 1.16b [90,91]. A packet consists of six variants with a parallel direction and a common close-packed plane of austenite, while a block within a packet comprises laths of variants belonging to the same Bain group, also parallel to the CP group.

Table 1.2. Bainite-austenite OR with ideal misorientation angle [92].

Orientation relationship	Parallel planes	Parallel Directions	Ideal Misorientation angle (°)
Bain	γ {100} ‖ α_b {100}	γ <100> ‖ α_b <110>	45
K-S	γ {111} ‖ α_b {011}	γ <110> ‖ α_b <111>	42.85
N-W	γ {111} ‖ α_b {011}	γ <112> ‖ α_b <011>	45.99

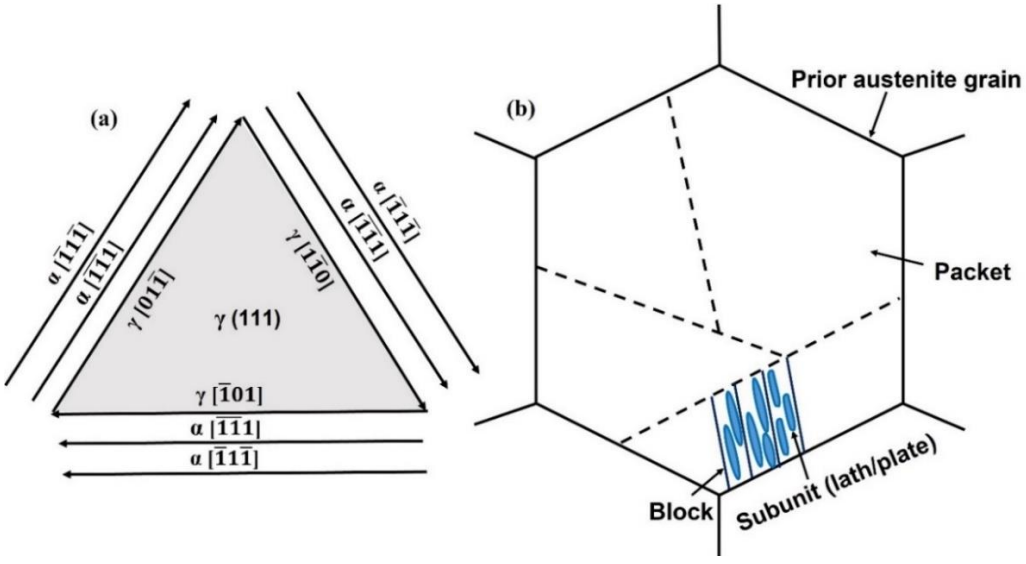

Figure 1.16. *Schematic diagrams (a) showing different variants for a single (111) close packed plane of austenite and (b) hierarchy in a prior austenite grain showing arrangement of packets, blocks and laths* [93].

While variant selection in bainite is similar to that of martensite[94], research on variant selection in nanostructured bainitic steel is relatively limited. The primary investigations on high carbon nanostructured bainite have been conducted by Beladi et al. [95,96] and on upper bainite by Furuhara et al. [89,94]. Both studies confirm the presence of strong variant selection at higher transformation temperatures (above 300 °C) and lower driving forces for transformation. Specific variants are favoured to minimize the transformation strain during bainite formation. The effect of transformation time on variant selection has been studied specifically for upper bainitic transformations [94,97]. However, limited study on OR of high carbon nanostructured bainite [95,96] shows N-W type relationship between bainite and austenite phase.

Table 1.3. Twenty-four variants of the K–S OR and corresponding CP and Bain groups [90].

Variant no.	Parallel plane	Parallel direction	CP-Group	Bain group	Misorientation from V1
V1	$\gamma\,(111)\,\|\|\,\alpha_b\,(011)$	$\gamma\,[\bar{1}01]\,\|\|\,\alpha_b\,[\bar{1}\bar{1}1]$	CP1	1	-
V2		$\gamma\,[\bar{1}01]\,\|\|\,\alpha_b\,[\bar{1}1\bar{1}]$		2	60
V3		$\gamma\,[01\bar{1}]\,\|\|\,\alpha_b\,[\bar{1}\bar{1}1]$		3	60
V4		$\gamma\,[01\bar{1}]\,\|\|\,\alpha_b\,[\bar{1}1\bar{1}]$		1	10.5
V5		$\gamma\,[1\bar{1}0]\,\|\|\,\alpha_b\,[\bar{1}\bar{1}1]$		2	60
V6		$\gamma\,[1\bar{1}0]\,\|\|\,\alpha_b\,[\bar{1}1\bar{1}]$		3	49.5
V7	$\gamma\,(1\bar{1}1)\,\|\|\,\alpha_b\,(011)$	$\gamma\,[10\bar{1}]\,\|\|\,\alpha_b\,[\bar{1}\bar{1}1]$	CP2	2	49.5
V8		$\gamma\,[10\bar{1}]\,\|\|\,\alpha_b\,[\bar{1}1\bar{1}]$		1	10.5
V9		$\gamma\,[\bar{1}\bar{1}0]\,\|\|\,\alpha_b\,[\bar{1}\bar{1}1]$		3	50.5
V10		$\gamma\,[10\bar{1}]\,\|\|\,\alpha_b\,[\bar{1}1\bar{1}]$		2	50.5
V11		$\gamma\,[011]\,\|\|\,\alpha_b\,[\bar{1}\bar{1}1]$		1	14.9
V12		$\gamma\,[011]\,\|\|\,\alpha_b\,[\bar{1}1\bar{1}]$		3	57.2
V13	$\gamma\,(\bar{1}11)\,\|\|\,\alpha_b\,(011)$	$\gamma\,[0\bar{1}1]\,\|\|\,\alpha_b\,[\bar{1}\bar{1}1]$	CP3	1	14.9
V14		$\gamma\,[0\bar{1}1]\,\|\|\,\alpha_b\,[\bar{1}1\bar{1}]$		3	50.5
V15		$\gamma\,[\bar{1}0\bar{1}]\,\|\|\,\alpha_b\,[\bar{1}\bar{1}1]$		2	57.2
V16		$\gamma\,[\bar{1}0\bar{1}]\,\|\|\,\alpha_b\,[\bar{1}1\bar{1}]$		1	20.6
V17		$\gamma\,[110]\,\|\|\,\alpha_b\,[\bar{1}\bar{1}1]$		3	51.7
V18		$\gamma\,[110]\,\|\|\,\alpha_b\,[\bar{1}1\bar{1}]$		2	47.1
V19	$\gamma\,(11\bar{1})\,\|\|\,\alpha_b\,(011)$	$\gamma\,[\bar{1}10]\,\|\|\,\alpha_b\,[\bar{1}\bar{1}1]$	CP4	3	50.5

V20		$\gamma\,[\bar{1}10] \,||\, \alpha_b\,[\bar{1}1\bar{1}]$		2	57.2
V21		$\gamma\,[0\bar{1}\bar{1}] \,||\, \alpha_b\,[\bar{1}\bar{1}1]$		1	20.6
V22		$\gamma\,[0\bar{1}\bar{1}] \,||\, \alpha_b\,[\bar{1}1\bar{1}]$		3	47.1
V23		$\gamma\,[101] \,||\, \alpha_b\,[\bar{1}\bar{1}1]$		2	57.2
V24		$\gamma\,[101] \,||\, \alpha_b\,[\bar{1}1\bar{1}]$		1	21.1

1.5.6 Stability of the retained austenite

The incomplete transformation phenomena explains that the complete transformation of austenite into bainite is not always possible. The retained austenite can be present in the material either in the form of blocky retained austenite (BRA) located between sheaves, or filmy retained austenite (FRA) present inside a sheaf, as illustrated in Figure 1.17. The presence of retained austenite in the material acts as a load-bearing phase and makes a significant contribution to the ductility and toughness. The transformation-induced plasticity (TRIP) effect is significantly influenced by the volume fraction, chemical stability, and morphology of the retained austenite [98]. Therefore, the stability of retained austenite is important from both thermal and mechanical standpoints [99].

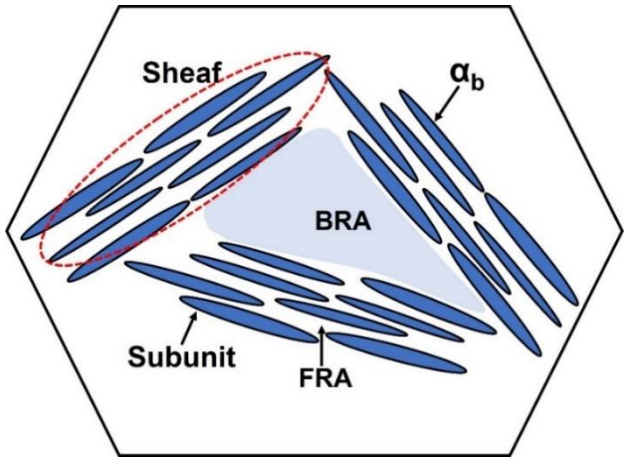

Figure 1.17. *Schematic diagram showing blocky retained austenite (BRA) and filmy retained austenite (FRA) in a prior austenite grain.*

The mechanical stability of RA primarily depends on the steel's chemical composition and its ability to resist martensite formation during deformation. Among various alloying elements, the concentration of carbon has a significant influence on the stability of

austenite. The filmy retained austenite contains a higher mass percentage of carbon compared to blocky retained austenite due to its isolation between bainite plates. The blocky morphology of austenite has a lower carbon concentration in the central region compared to the bainite-austenite interface due to limited diffusion distance. This constrained carbon concentration proves detrimental to toughness since austenite transforms non-uniformly into martensite during deformation [100]. In contrast, thin austenite is more stable and persists in an untransformed state during subsequent stages of deformation. This stability arises from the suppression of the strain-induced martensite start temperature and the continuous presence of high-carbon retained austenite [101,102]. The ratio of filmy to blocky retained austenite should exceed approximately 0.9 for optimum properties, as suggested by Bhadeshia and Edmonds in Equation 1.4 [65].

$$\left(\frac{V_{\gamma f}}{V_{\gamma b}}\right) = \frac{V_{\alpha_b}}{(6-7.7V_{\alpha_b})} > 0.9 \qquad (1.4)$$

Where V_{α_b} is the volume fraction of bainite, $V_{\gamma f}$ and $V_{\gamma b}$ are the volume fractions of filmy and blocky morphologies respectively. A higher volume fraction of austenite is likely to have a diminished carbon concentration, while a considerably lower amount of austenite could possess such a high carbon content that it remains untransformed altogether [98].

In early studies on transformation-induced plasticity (TRIP)-aided steels, the improved elongation was attributed to the strain-induced martensitic transformation of retained austenite during tension [103,104]. However, a calculation conducted by Bhadeshia [105] revealed that only 2% of the ductility is contributed by the austenite-to-martensite transformation, which is a small portion compared to the total value of about 15-30%. Recent research has highlighted the contribution of microconstituents other than austenite in the overall deformation behaviour. [105–107].

During deformation, strain initially concentrates in the softer phase, such as austenite [108,109]. Harder phases like bainite or martensite undergo plastic deformation only after the

softer constituents have strain hardened. The fraction of RA can transform into martensite during uniaxial loading through either stress-assisted or strain-induced mechanisms, depending on the alloying elements present in the RA and its morphology. The martensite transformation occurring after yielding is known as strain-induced transformation, while the transformation occurring before yielding is referred to as stress-induced martensitic transformation [110,111]. The presence of harder phases reduces the mean stress in the austenite, thereby delaying the strain-induced martensitic transformation. This progressive transformation process is beneficial for enhancing ductility.

The thermal stability of austenite is also crucial for the high-temperature applications of materials and is closely related to the tempering process in steel. During tempering, the material is heated to elevated temperatures (ranging from 150°C to 700°C) in order to improve properties such as ductility and toughness for specific applications [112]. Steels that contain martensite are typically subjected to tempering treatment, for around 1 hour, to relieve internal stresses generated during rapid cooling from the austenite phase. This tempering process helps alleviate the internal stresses at the expense of a slight reduction in strength and hardness.

During tempering, steel parts are typically heated isothermally at a specific temperature and then cooled in still air. This process allows for the controlled relaxation of internal stresses and the desired modification of mechanical properties in the material. The mechanism and structural changes produced by tempering are grouped in four stages as follows [113,114] :

• Stage I (up to 200 °C): Diffusion and segregation of carbon and the lowering of the carbon content in the martensite.

• Stage II (200-400 °C): The transformation of retained austenite to lower bainite and formation of transition carbides like epsilon (ε).

• Stage III (400-600 °C): The replacement of transition carbide and low carbon martensite by cementite and ferrite.

• Stage IV (above 600 °C): Cementite particles are coarsened and the development of alloy carbides or secondary hardening in alloy steels.

There are notable differences in the tempering behaviour between bainite and martensite. The bainitic transformation typically occurs at higher temperatures compared to martensite, which promotes auto-tempering during isothermal holding. Bainite tempering is less sensitive to small variations in carbon content compared to martensite. In martensite, the strength and hardness decrease rapidly as carbon leaves the solid solution.

However, in bainitic steels, the primary source of strength comes from the thickness of subunits rather than the carbon content within them [75]. As a result, nanostructured bainite exhibits the ability to resist tempering effects up to temperatures around 500 °C without significant changes in hardness. This is due to the strong contribution of the subunit thickness to the overall strength of bainite, which helps maintain hardness even during tempering. During the tempering of bainite, carbide precipitation primarily occurs in the bainitic ferrite region, where the driving force for precipitation is the highest [75]. Bainitic steels have a high dislocation density, resulting in more carbon being trapped in Cottrell atmospheres and not being readily available for initial carbide precipitation [115]. As a result, the driving force for carbide precipitation is reduced, and cementite is more likely to precipitate directly. However, in materials with moderate dislocation density, cementite precipitation occurs via the formation of transition carbides, such as epsilon (ε) carbide. Epsilon carbide has a hexagonal structure with the chemical formula $Fe_{2.4}C$ [116]. Cementite nucleates either independently or on the surface of epsilon carbide particles and consumes the epsilon carbide as it grows.

1.5.7 Tensile properties of nanostructured bainite

In a polycrystal, the application of stress causes dislocations to move within a grain if the stress exceeds the critical resolved shear stress for that particular grain. However,

dislocations cannot cross grain boundaries, so they accumulate at the boundaries until the stress is high enough to induce slip in an adjacent grain. At this point, plastic deformation can occur, and the material is said to have yielded. For polycrystals with equiaxed grains of micron size, the yield stress (σ_o) is related to the grain size (d) by the Hall-Petch relation, given by Equation 1.3.

But the Hall-Petch equation cannot accurately predict the strength of nanostructured materials because pile-up is not possible on a slip plane for grain sizes smaller than 1 μm. In these materials, yielding occurs through the expansion of dislocation loops [117]. The yield strength of nano bainitic steel (σ_y) is mainly contributed by nano-sized plates and relates with dislocation density in bainite as given by Equation 1.5 [73,118].

$$\sigma_y = \sigma_{Fe} + \sigma_{ss} + \sigma_c + k_p(t_b)^{-1} + 7.34 \times 10^{-6}\rho^{1/2} \qquad (1.5)$$

Where σ_{Fe} is the frictional strength of pure iron in the annealed condition, σ_{ss} denotes the solid solution strengthening from substitutional elements, σ_c represents the strengthening contribution due to carbon, k_p is a fitting parameter with a calculated value of 115 MPa [102]. Among these factors, the average thickness of bainite plates and dislocation density in bainite significantly contribute to the overall strengthening [83]. The plate thickness shows an inverse relationship with strength [117], while the dislocation density directly relates to it [119]. Garcia-Mateo and Caballero [120] conducted mechanical testing and attributed the strengthening to contributions from the plate size and the dislocation density. Dislocation density is measured from the peak broadening in X–ray diffraction experiments and plate thickness measured using transmission electron microscopy.

Bhadeshia and Edmond [65] demonstrated that the presence of a soft phase like retained austenite (RA) contributes to improved ductility and toughness by reversing crack movement. Additionally, the addition of silicon helps restrict cementite precipitation, which can act as a

crack initiation site. The importance of retained austenite for ductility improvement has also been reported by Garcia-Mateo et al. [121,122]. In another study, the authors concluded that the extended work hardening resulting from the presence of retained austenite contributes to higher ductility in bainitic steel [123]. In order for strain hardening to effectively contribute to ductility, austenite should possess moderate stability. Highly stable austenite will not transform to martensite at all, while low stability of martensite will result in a lower extent of work hardening. Similarly, austenite should maintain a continuous path in the material during strain-induced martensitic transformation.

1.5.8 Work hardening behaviour

The ductility of bainitic steel mainly depends on its strain/work hardening behaviour, which is indirectly affected by the stability of RA. In this context, the stability of RA is related to its mechanical stability, which refers to its ability to resist the formation of martensite during deformation. To achieve better strain hardening, the formation of martensite should not occur too early or too late [123,124] . The formation of martensite from retained austenite depends on two major factors: carbon content and the morphology of RA [124]. Very high carbon content can lower both the thermal and deformation-induced martensite start temperature, resulting in partial transformation of austenite during deformation. Similarly, too low carbon content will increase the martensite start temperature, and early deformation-induced martensite formation can lead to failure [121]. The two types of austenite morphology mentioned earlier [82], can affect strain hardening due to the accumulation of more carbon in filmy retained austenite, and less inhomogeneous in blocky retained austenite. Although FRA is advantageous compared to BRA, as pointed out by many researchers [125–127], the quantity of carbon still plays a major role in controlling different mechanical properties.

The work hardening behavior of a low carbon bainitic steel [128] exhibits three stages of slope change. In stage I, the austenite phase, being the softer phase, initially deforms uniformly, showing the lowest slope change. In stage II, there is a strain-induced martensitic transformation from RA, leading to prolonged strain hardening in this stage. In stage III, all phases (bainite, martensite, and retained austenite) deform simultaneously, resulting in the highest slope in the work hardening plot (Fig. 1.18).

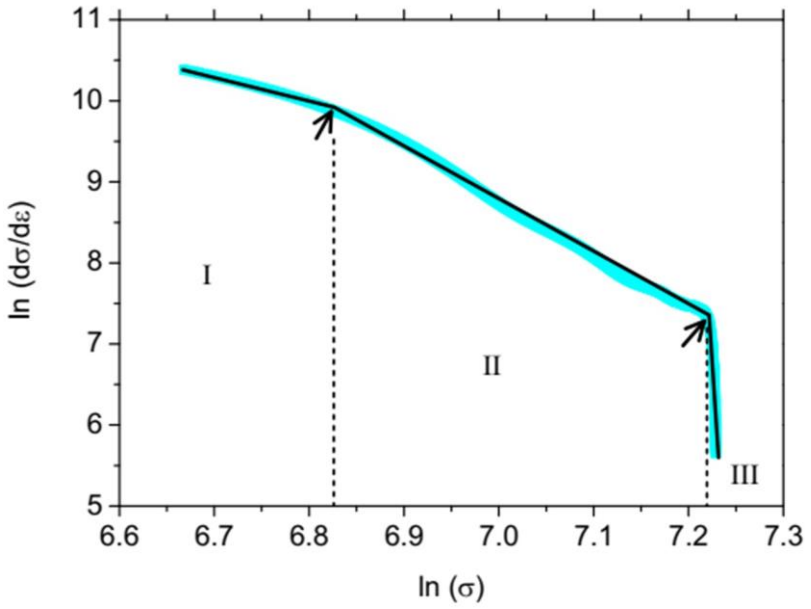

Figure 1.18. *Rate of work hardening plot showing different stages of hardening in a low carbon bainitic steel* [128].

1.5.9 The incomplete-reaction phenomenon (T_0 and T_0' Concept)

In Si-containing bainitic steels, when the appropriate amount of carbon is present in the RA, the material is free from carbides, allotriomorphic ferrite and martensite. The growth of bainite in these steels occurs through a diffusionless mechanism and requires a temperature below T_0 and the free energy of bainite is below that of austenite of same composition (Fig. 1.19a) [129]. The T_0 temperature is obtained for a particular carbon concentration, where free energy of ferrite and austenite are equal. The locus of the T_0 temperature as a function of the carbon concentration is referred as T_0 curve. The energy stored in the form of elastic strains in

the case of bainite, amounts to $G_{SB} \simeq 400$ Jmol^{-1}. The strain energy due to transformation raises stored energy of bainitic ferrite, giving the T_0' curve as shown in the Figure.1.19a. The extra carbon in the bainite partitions into the remaining austenite after growth stage, forcing the subsequent plate to develop from carbon-enriched austenite [75]. The process eventually comes to an end as the austenite carbon content reaches T_0' value, known as the incomplete reaction phenomenon [54]. It is important to note that this theory applies only to Si-containing bainitic steels without carbides and does not apply to steels that form carbides. The maximum fraction of bainite (V_b^{max}) at any temperature can be determined by lever-rule as given in Equation 1.6 [130].

$$(V_b^{max}) = \frac{C_{T_0'} - \bar{x}}{C_{T_0'} - x_{\alpha_b}} \qquad (1.6)$$

where $C_{T_0'}$ is the austenite carbon content given by the T_0' boundary, $\bar{x}$ is the alloy average carbon concentration and x_{α_b} is the carbon concentration of the bainitic ferrite. The thermodynamic restriction imposed by the T_0' curve on the amount of bainite transformation can lead to formation of retained austenite with a blocky morphology.

From Figure 1.19b, it is evident that transformation at higher temperatures results in less bainite formation as the T_0' carbon concentration is reached earlier. Additionally, at higher austempering temperatures, there is a formation of coarse bainite plates. On the other hand, lower austempering temperatures promote higher amount of bainite formation of smaller plate thickness. However, lower austempering temperatures also lead to slower transformation kinetics. To accelerate bainite transformation kinetics, various methods can be employed, which will be discussed in the subsequent sections.

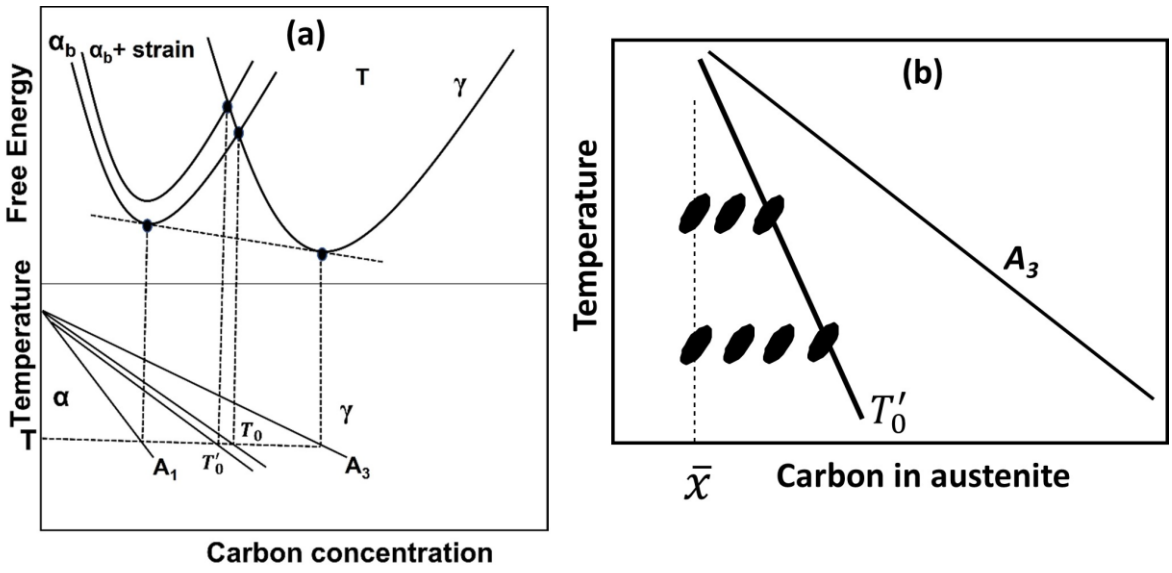

Figure 1.19. *Schematic illustration of the T_0 and T_0' curves . T is the temperature corresponding to the free energy curves* [119].

1.5.10 Acceleration of bainitic transformation

There are several methods that can be employed to improve the kinetics of bainitic transformation. These include alloy modification [131,132], the application of a magnetic field [133,134] and the introduction of deformation [135,136]. Alloy modifications involving the addition of cobalt and aluminium have been found to accelerate bainitic transformation by increasing the driving force[131]. However, these alloy additions alone cannot achieve the level of acceleration of transformation required for industrial applications. The application of a magnetic field during the transformation process can lead to the formation of undesired elements like pearlite, and the requirement of high magnetic field strengths exceeding 10 T limits its practical use. While some reports suggest that up to 15% deformation can accelerate the transformation, other studies suggest that the kinetics may be slowed down due to the stabilization of retained austenite[137,138]. Bhadeshia and his colleagues have suggested that in the early stages of transformation, deformation accelerates bainitic transformation, while in the later stages, it can retard the process due to strain hardening [139,140]. In general, these studies indicate that high levels of strain decrease the rate of transformation, and lower amounts

of strain can accelerate it. However, the overall conclusion is that the transformation process remains complex, and significant reduction in transformation time has not been achieved.

1.6 Acceleration of phase transformation by electropulsing

1.6.1 Thermodynamic effects

Electropulsing (EP) can alter the thermodynamic and kinetic properties of phase transformation as discussed below. Thermodynamic effect investigated by Dolinsky and Elperin [141] demonstrate that, phases with higher conductivity are promoted in a current carrying wire with shifting of equilibrium line between two phases. If a nucleus is formed from a current carrying conductor, the work (W_f) in this process is given by the Equation 1.7 [141].

$$W_f = \mu g \xi V I^2 \qquad (1.7)$$

The symbol μ denotes magnetic susceptibility, which is taken in vacuum (μ_0), g is a geometric factor depends on radius of conductor, V is the volume of nucleus formed and I is the current density. The symbol ξ depends on electrical conductivity of the material as given by the Equation 1.8 [141].

$$\xi = \frac{\sigma_1 - \sigma_2}{\sigma_2 + 2\sigma_1} \qquad (1.8)$$

Here σ_1 and σ_2 are electrical conductivities of initial phase and nucleating phases respectively. It is clear from the Equation (1.8) that, for nucleation of a higher conductive phase ξ will be negative and hence the W_f.

Nucleation rate (I_e) in a current carrying system can be expressed by the Equation 1.9 [47,142]

$$I_e = I_0 \left(\frac{D}{\lambda^2}\right) exp\left(-\frac{\Delta W_0 + \Delta W_f}{kT}\right) \qquad (1.9)$$

Where I_0 is the nucleation rate of the current-free system, D is the diffusivity, λ is the atomic jump distance, ΔW_0 is the Gibbs energy change in the current-free material and ΔW_f is the

Gibbs energy change in the current carrying system. It is clear from Equations 1.8 and 1.9 that, for the nucleation of higher conductive phases Gibbs energy change will be negative, which can increase nucleation rate as shown in Equation 1.9.

The resistivity versus temperature plot of different phases in steel (Figure 1.20) [75] reveals that austenite has the highest resistivity or lowest conductivity among the various phases, followed by martensite, bainite, and ferrite. Therefore, during the passage of electrical current, the lower conductive phase should transform into the higher conductive phase, such as bainite, rapidly, as observed from the theories discussed earlier. This phenomenon occurs due to the higher conductivity of bainite compared to austenite, promoting the transformation towards a phase with better electrical conductivity.

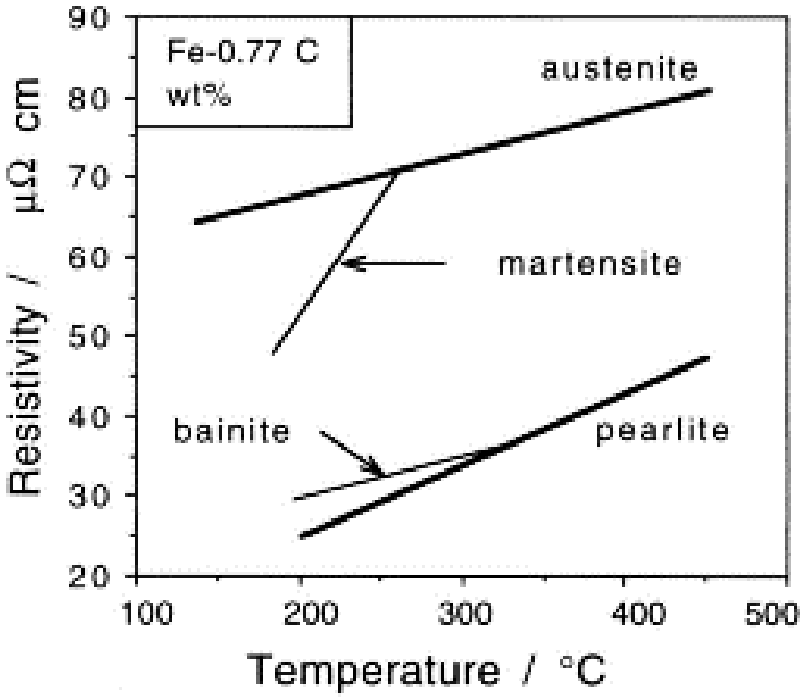

Figure 1.20. *Resistivity vs. temperature plot of different phases in steel* [75].

1.6.2 Kinetic effects

Kinetic effect of EP is described mainly based on migration of atoms. Different factors contributing towards accelerated atomic diffusion is given by Nernst – Einstein equation (1.10) [143,144].

$$J = J_c + J_e = D_i\left(-\frac{\partial C_i}{\partial x}\right) + C_i\frac{D_o}{kT}exp\left(\frac{E_a}{kT}\right)Z^*e\rho_r I \qquad (1.10)$$

Here J_c is the diffusion flux due to concentration gradient and J_e is the diffusion flux caused due to current. C_i is the vacancy concentration, D_0 is the pre-exponential diffusion factor, k is the Boltzmann constant, Z^* is the effective charge, T is the absolute temperature, e is the charge of electron, ρ_r is the electric resistivity, and I is the current density.

The movement of atoms within a material is accelerated in the presence of a current pulse, and the current density has a significant effect on this acceleration. This phenomenon has been confirmed in early studies conducted on bearing steel [144] . Specifically, it has been observed that a sample treated at 750 °C for 0.5 hours exhibits a high concentration of carbides (Figure 1.21a). However, when an electric current pulse is applied during heating at the same temperature, the carbides dissolve, as observed in the SEM bright field image shown in Figure 1.21b. This indicates that the application of the electric current pulse promotes the dissolution of carbides within the material.

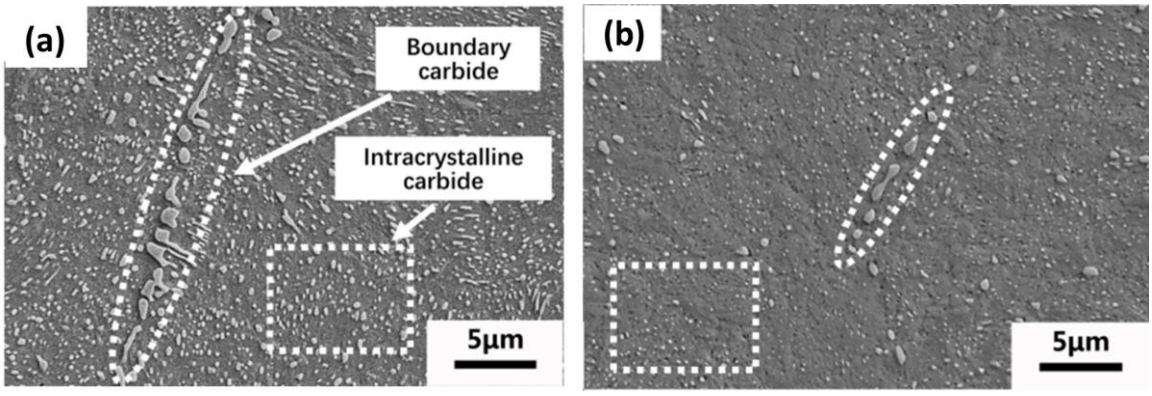

Figure 1.21. *SEM micrographs of the sample quenched after (a) heat treatment for 0.5 h at 750 °C, (b) electropulsing at a current density of 80 Amm^{-2} for 0.5 h* [144].

The application of a high-density current pulse (I=5.67 x 10^9 Amm^{-2}) to a dual-phase steel (Figure 1.22a) for a pulse duration of 110 μs results in the formation of ferrite and the precipitation of cementite within the martensite phase (Figure 1.22b) [145]. Although the temperature rise reaches approximately 685 °C, the precipitation of cementite is believed to be the combined effect of both thermal effects (Joule heating) and athermal effects (electron wind force) induced by the high-density current pulse. These combined effects contribute to the observed precipitation of cementite within the martensite phase.

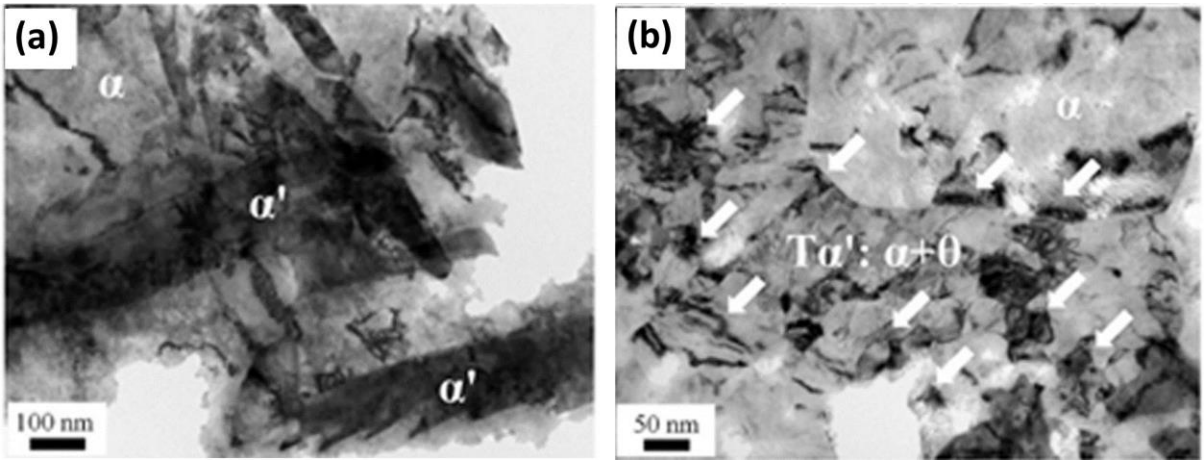

Figure 1.22. *TEM BF images of dual phase steel (a) before EP and (b) after EP. (α denotes ferrite, α' denotes martensite and θ is cementite)* [145].

1.7 Motivation

- Electropulsing has the potential to eliminate nonequilibrium boundaries and increase dislocation activity in ultrafine-grained materials processed by SPD techniques, thereby enhancing their ductility.
- Limited research has been conducted on the defect structure and crystallographic variant evolution in bainitic steel during austempering in high carbon low alloy steels.

- Influence of dislocation density within the retained austenite phase on the thickness of bainite plates, at longer austempering times is not clearly explored.
- Strain hardening due to transformation induced plasticity is one of the factors for the ductility of bainitic steel. However, it is not studied for high carbon steel containing higher amount of RA.
- Electropulsing has the potential to accelerate the kinetics of bainitic transformation by promoting carbon diffusion during nucleation, caused by low austempering temperature.
- There is a possibility of finer scale of carbide precipitation in martensite and additional transformation of retained austenite driven by electropulsing.

1.8 Objectives of the present investigation

- The effect of electropulsing on ultrafine-grained ferritic steel processed by Equal-channel angular pressing.
- Design of suitable steel composition to achieve nano-structured bainite with minimum carbide content.
- The influence of different austempering durations on the microstructural evolution of nanostructured bainite in the selected steel.
- Effect of austempering time on variant selection of nanostructured bainite in the steel.
- Strain hardening behavior of high carbon low alloy bainitic steel containing different amounts of retained austenite.
- The impact of electropulsing on the microstructural stability of retained austenite, bainite, and martensite in the high carbon low alloy steel.